Journal of Materials Chemistry C

ROYAL SOCIETY OF CHEMISTRY

COMMUNICATION

View Article Online
View Journal | View Issue

Cite this: J. Mater. Chem. C, 2021, 9, 3396

Received 4th January 2021,
Accepted 15th February 2021

DOI: 10.1039/d1tc00042j

rsc.li/materials-c

A deep-dyeing strategy for ultra-stable, brightly luminescent perovskite-polymer composites†

Caicai Zhang,‡[ab] Zigian He,‡[c] Mirra Mogensen,[d] Andre J. Gesquiere,[cd] Chia-Hsun Chen,[e] Tien-Lung Chiu,[f] Jiun-Haw Lee,[g] Shin-Tson Wu*[c] and Yajie Dong *[abc]

To fulfill the requests of highly vivid colors in displays and customized spectra in solid-state lighting (SSL), a cost-effective approach to create color-tunable downconverters with narrow emission spectra is in demand. In this regard, perovskite nanocrystal downconverters have aroused great interest due to their narrow-band, tunable emission and easy manufacturing process. However, environmental instability is still the major concern of their commercialization, especially for red-emitting downconverters. Herein, built upon the previous successful development of a swelling–deswelling microencapsulation (SDM) method, we report a deep-dyeing strategy that can directly convert commercial solvent-resistant polymer matrices (*e.g.* polyethylene terephthalate (PET)) into polymer-protected deep-dyed perovskite polymer composites (DDPPCs) with outstanding color tunability, excellent pure color, and superior environmental stability. The $MAPbBr_3$-based DDPPCs manifest a high photoluminescent quantum yield of 77.9%. Moreover, they survived in water for over 3 years without visible degradation, their photoluminescence (PL) is reversible under a 140 °C heating–cooling cycle, and they maintained 87.6% of the original PL intensity after 10 hours of continuous blue laser excitation. More importantly, the as-synthesized $CsPbBr_{0.75}I_{2.25}$-based red DDPPCs also exhibit excellent water-, thermal-, and photo-stability. The deep-dyeing process is expected to achieve highly stable PPCs for next-generation displays, SSL or other applications.

1. Introduction

The recent advances of displays have set a higher goal for more vivid colors which traditional phosphor-based color conversion materials can hardly meet.[1–3] Meanwhile, future solid-state lighting (SSL) systems call for customized spectra to maximize the energy utilization efficiency for specific applications.[4–7] Incorporating novel downconverter materials of high tunability and narrow emission peaks with blue light emitting diodes (LEDs) is generally considered the most efficient and cost-effective approach.[8–11] Among the emerging downconverters, quantum dots have been intensively investigated and shown promise for saturated color emission and fine spectrum control, yet their high cost and relatively poor stability still limit their wide adoption in the display and lighting industries.[12–15]

Meanwhile, metal halide perovskite (MHP) nanoparticles have attracted great attention as highly promising, emerging optoelectronic materials. MHPs usually have the chemical formula of ABX_3, where typically X is a halide anion (I^-, Br^-, Cl^-, F^-), B is lead (Pb^{2+}), and A is Cs^+, MA^+ ($CH_3NH_3^+$) or FA^+ ($CH(NH_2)_2^+$).[16–18] MHP materials, especially with nanocrystal (NC) forms, have demonstrated high luminescence efficiency, narrow bandwidth, and excellent color tunability that covers the entire visible band by simply tuning the halide compositions.[19–23] Despite all of these developments, the main obstacle for perovskite materials to be vastly applied in industry is their instability under external environmental stimuli, such as heat, light, moisture or oxygen exposures.[24–28]

To solve this issue, a strategy termed swelling–deswelling microencapsulation (SDM) has been reported by our group in 2016. By solvent-induced swelling, perovskite precursors will swell the polymer chains and will be introduced into the matrices. Followed by a polymer deswelling process/solvent

[a] NanoScience Technology Center, University of Central Florida, Orlando, Florida, 32826, USA. E-mail: Yajie.Dong@ucf.edu
[b] Department of Materials Science & Engineering, University of Central Florida, Orlando, Florida 32816, USA
[c] College of Optics and Photonics, University of Central Florida, Orlando, Florida 32816, USA
[d] Department of Chemistry, University of Central Florida, Orlando, Florida 32816, USA
[e] Department of Chemistry, National Taiwan University, Taipei 10617, Taiwan
[f] Department of Electrical Engineering, Yuan Ze University, Taoyuan 32003, Taiwan
[g] Graduate Institute of Photonics and Optoelectronics and Department of Electrical Engineering, National Taiwan University, Taipei 10617, Taiwan

† Electronic supplementary information (ESI) available. See DOI: 10.1039/d1tc00042j

‡ These authors contributed equally.

removal, well-dispersed perovskite nanoparticles are formed and encapsulated inside the polymer matrices so that the as-synthesized perovskite nanocrystals (NCs) can be protected by the polymer matrices and the stability can be enhanced.[29–32] This strategy is easy to process and low cost, and the achieved composites manifest high photoluminescent (PL) efficiency, outstanding color purity with narrow bandwidth and superior thermal and water stability.[33,34] In the initial work, only pure-bromide based perovskite-polymer composite (PPC) films were presented due to the fact that other halide compositions resulted in either poor stability or dimmed luminescence. In a later work, we studied how ligands helped with further stabilizing perovskite NCs in the SDM strategy.[35,36] Attributed to the use of ligands, environmentally stable PPC films emitting different colors were achieved by tuning the halide compositions.[37]

Even though previous works have already realized high efficiency green PPCs with outstanding stabilities, efforts are still needed to further boost their stability for practical applications.[38,39] Moreover, even with the help of ligands, the red PPCs are still not as bright and stable as green PPCs especially under intense environmental stress, which is previously considered as the perovskite "red wall" issue. The issue refers to the structural instabilities of iodine-containing perovskite NCs emitting red to near-infrared spectral ranges.[40] To crack the "red wall" and better protect the vulnerable iodine-based perovskite NCs from harsher environments, an even more stable polymer matrix with better barrier properties is in demand. Therefore, poly(ethylene terephthalate) (PET) attracts our attention, as it has been widely used as a barrier film owing to its low penetration rate of oxygen and moisture, and excellent mechanical properties.[41,42] However, because commercial PET is normally prepared with high crystallinity and lacks reactive groups, its swelling ratio at room temperature is fairly low and thus it can hardly be converted into PPCs through the previously reported SDM strategy.[43–46]

Herein, we develop an advanced version of the SDM method, termed deep-dyeing strategy,[47–49] which is able to convert inert, solvent-resistant polymer matrices into bright, ultra-stable PPCs.[50–54] Choosing PET as the typical solvent-resistant polymer matrix, the deep-dyed perovskite-polymer composites are realized. Based on the evaluation and characterization, the obtained DDPPCs offer highly saturated and widely tunable emission colors. The composites also show outstanding stability against external stress, indicating their great potential to be employed as a high-quality, low-budget option to replace the traditional, high-budget downconverters in industrial applications such as displays, SSL and beyond.

2. Results and discussion

The previously published SDM method is suitable for a series of polymer matrices swellable at room temperature, including polystyrene, polycarbonate, cellulose acetate, and so on. However, for more sturdy polymer matrices such as PET, the polymer swelling ratio at room temperature is fairly low and PPCs cannot be generated by the regular SDM method. Herein, a deep-dyeing process is proposed to convert inert polymer matrices into bright and stable PPCs. In this process, the temperature is high enough to swell the PET matrix and open the polymer chains. As shown in Scheme 1, typical PET matrices with different form factors, such as sheets or fibers, are first immersed in the prepared MHP precursor solution. Note that the precursor solution also contains a mixture of surfactants including octylamine (OcA)/oleic acid (OA) or oleylamine (OAm)/OA (experimental details can be found in the ESI†). Then the solution is heated to a relatively high temperature (*e.g.* 160 °C) to swell the PET polymer chains, allowing the solvent and solute to enter the interior. After the solution is cooled to room temperature, a follow-up deswelling drying process (*e.g.* annealing or antisolvent washing) is applied to drive out the solvent. During this deswelling process, perovskite NCs are uniformly formed inside the polymer, and the PET polymer chains shrink, thereby protecting the embedded perovskite NCs. After sufficient drying (*e.g.* 80 °C baking for 2–6 hours), the luminescent DDPPCs are obtained.

In this deep-dyeing process, temperature control, high-temperature swelling time, choice of antisolvent, antisolvent deswelling time, and baking process are key factors for the development of uniform, ultra-stable DDPPCs.

As shown in Fig. S1 (ESI†), during the swelling process, if the operating temperature is not high enough (*e.g.* 130 °C), or the heating time is too short (*e.g.* 0.5 h), the firm PET chains will not be sufficiently swelled by the solvent. Or *vice versa*, when the operating temperature is too high (*e.g.* 190 °C), or the heating time is too long (*e.g.* 1.5 h), the PET polymer chains

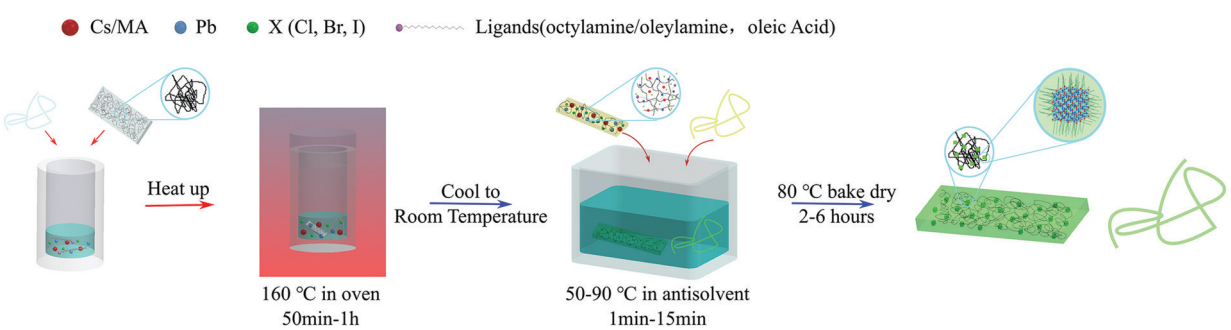

Scheme 1 Fabrication workflow of the deep-dyeing SDM strategy for achieving ultra-stable DDPPCs.

can be destroyed and the matrices can be dissolved by the solvent.

The baking–deswelling process is also pivotal. Although directly using a heat gun to dry the swelled composite without using an antisolvent can lead to bright DDPPCs, the PL uniformity is hard to control due to the perovskite degradation and PET polymer deformation under local high temperature drying, as depicted in Fig. S2 (ESI†). To create uniform DDPPCs, a two-step process has been developed. First, the swelled composite is immersed in an antisolvent to form perovskite NCs uniformly inside the matrix. Then, an 80 °C baking slowly shrinks the PET polymer chains, protecting the as-formed NCs without significant thermal degradation. This low temperature baking process is crucial, otherwise the as-synthesized perovskite NCs cannot be fully protected by the matrix (Fig. S3, ESI†).

In the deswelling process, the choice of antisolvent can affect the uniformity of DDPPCs, as described in Fig. S4 (ESI†). Isopropyl alcohol (IPA) is a common antisolvent with minimum environmental safety concerns. Using IPA as the antisolvent, however, the uniformity of the DDPPCs is relatively poor, and varies as a function of immersing time in this case. If toluene is used as the antisolvent instead, more uniform DDPPCs can be easily obtained, and the immersion time is less sensitive. Our observation matches with the previous report that an antisolvent with a lower dielectric constant is more effective in extracting solvent from the perovskite precursors and forms more uniformly dispersed perovskite nanoparticles.[55] With careful controls, the process is universal and applicable to a series of MHP precursor solutions (perovskite as $MAPbX_3$ or $CsPbX_3$) with specific halide components (X = I, Br, Cl) to realize widely tunable bandgaps, as presented in Fig. 1a–f. DDPPCs with 2D and 1D form factors are synthesized through halide composition modification, where saturated colors can be recognized under UV excitation. As assumed, the $CsPbBr_3$ or $MAPbBr_3$ DDPPCs exhibit green emission. By tuning the ratio of $PbCl_2$ or PbI_2 to $PbBr_2$, the emission peak can be blue-shifted or red-shifted, respectively. The thickness of the obtained DDPPC films is also tunable depending on the thickness of the original PET films. For example, 80 μm and 30 μm DDPPC films are achieved, as shown in Fig. S5 (ESI†). Fibers with different diameters (*e.g.* 20 μm) can also be converted to DDPPC fibers, as illustrated in Fig. S6 (ESI†). The versatile tunability indicates a wide range of potential application scenarios.

Microscopic characterizations are conducted to prove the good uniformity of perovskite NCs inside the polymer matrices. From Fig. 1g and h, both $CsPbBr_3$ and $CsPbBr_{0.75}I_{2.25}$ NCs are uniformly distributed over the field of view and no particle-like features are observed when changing the focus across the film. Fig. 1i demonstrates a cross-sectional transmission electron microscopy (TEM) image of the $CsPbBr_3$ DDPPCs, which further confirms the good dispersion of crystalline nanoparticles inside the matrices. The uniform distribution of NCs with other compositions can also be observed in Fig. S7 (ESI†). The high resolution TEM (HRTEM) (Fig. 1j) image and its fast Fourier transformation (FFT) image (Fig. 1k) indicate the interplanar distances of ~1.88 and ~4.01 Å, which are close to (103) and ($\bar{1}$10) crystal planes of the monoclinic $CsPbBr_3$ crystal (PDF#18-0364). The angle between the two planes should be 102.9°, which is also similar to the result (100°) calculated from Fig. 1j. As seen in Fig. S8 (ESI†), the crystal structure of $CsPbBr_{0.75}I_{2.25}$ NCs is analysed. The HRTEM and FFT images indicate the interplanar distances of ~5.98 and 4.83 Å, which are proportional to the (012) and (020) crystal faces of the orthorhombic $CsPbI_3$ crystal (PDF#18-0376). The

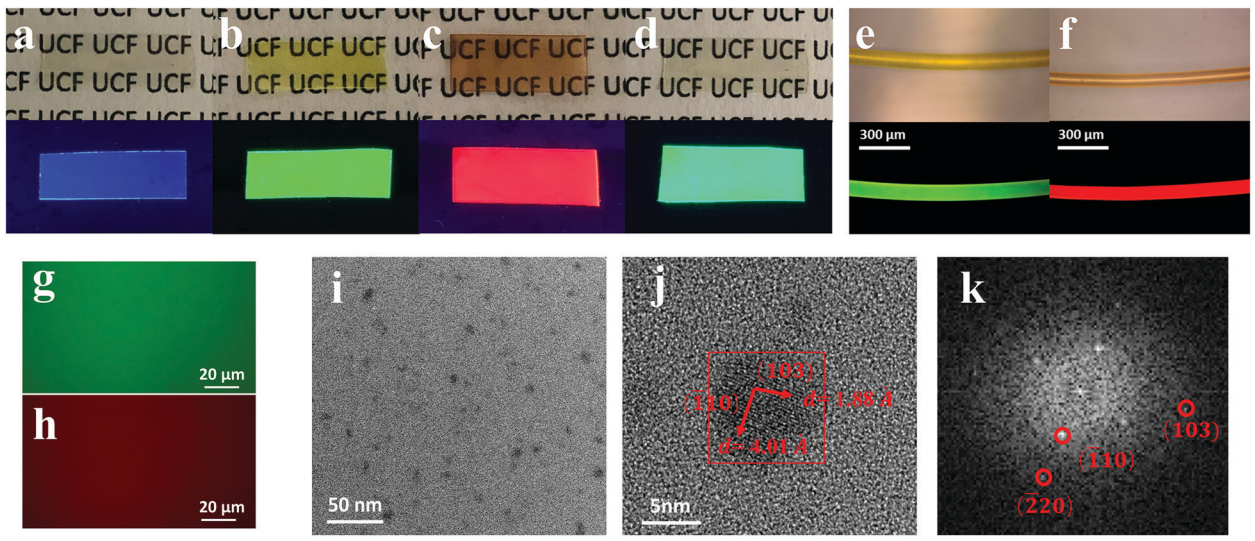

Fig. 1 Characterizations of DDPPCs fabricated by the deep-dyeing strategy. (a–d) Photos of 80 μm thick DDPPC films under ambient (top) and 365 nm UV (down) excitation with perovskite compositions of (a) $CsPbCl_1Br_2$, (b) $CsPbBr_3$, (c) $CsPbBr_{0.75}I_{2.25}$, and (d) $MAPbBr_3$. (e and f) Bright field (top) and fluorescent (down) optical microscope images of 80 μm diameter DDPPC fibers with perovskite compositions of (e) $MAPbBr_3$ and (f) $CsPbBr_{0.75}I_{2.25}$. (g and h) Fluorescence optical microscope images of DDPPC films with perovskite compositions of (g) $CsPbBr_3$ and (h) $CsPbBr_{0.75}I_{2.25}$. (i) The cross-section TEM image of the $CsPbBr_3$ DDPPC film. (j) The HRTEM image of $CsPbBr_3$ NCs shown in (i). (k) FFT of (j).

angle between the two planes should be 63.4°, which is also well fitted in the HRTEM image. Fig. S9a (ESI†) presents the HRTEM image of $MAPbBr_3$ DDPPCs, where no obvious crystal structure is detected through individual $MAPbBr_3$ NCs. In fact, the crystal structure of MA-based perovskites is not as distinctive as that of Cs-based perovskites. The noise from the polycrystallinity PET matrix will make the characterization even harder. Fortunately, through X-ray diffraction (XRD) characterization (Fig. S9b, ESI†), some characteristic peaks of $MAPbBr_3$ can be recognized, even though the noise from the PET matrix still dominates.

Further optical characterizations demonstrate that DDPPCs have outstanding color purity, color tunability, and optical density control capability. PL spectra and the corresponding UV-vis absorption spectra of the DDPPC films are shown in Fig. 2. The PL emission peaks can be adjusted from short wavelength blue (477 nm) to long wavelength red (645 nm) with the full width at half maximum (FWHM) ranging from 18 nm to 42 nm. Interestingly, the amount of ligands can affect the emission peak wavelength and bandwidth of DDPPCs, as demonstrated in Fig. S10–S12 (ESI†). Overall, increasing the amount of ligands causes blue shifts of the emission peak, consistent with what has previously been observed for colloidal perovskite nanoplates.[37,56,57] On the other hand, the optical density of DDPPCs can also be well controlled by tuning the perovskite precursor concentration from 0.04 M to 0.01 M, as shown in Fig. S13 (ESI†). A higher precursor concentration leads to a higher NC loading, and thus a larger optical density. PL spectra of green and red emitting DDPPC fibers are also recorded, as depicted in Fig. S14 and S15 (ESI†). Among all the synthesized DDPPCs, the green emitting $MAPbBr_3$ DDPPC manifests the highest photoluminescent quantum yield (PLQY) of 77.9%. The detailed emission peaks, FWHMs and PLQY data of some synthesized DDPPCs are listed in Table 1.

Longer PL lifetimes generally indicate good perovskite NC quality and better performing films.[24,58] According to previous reports, the average PL lifetimes (τ_{avg}) of $MAPbBr_3$-based films or colloidal nanoparticles are usually within 10–100 ns.[24] For $MAPbBr_3$-polymer composite films prepared with the previous SDM method, they showed τ_{avg} ranging from 130 ns to 502 ns.[34] In the studies reported here, the $MAPbBr_3$-PET DDPPC film shows τ_{avg} of ~2000 ns (Table S1, ESI†), which is much longer than the previous ones. The $CsPbBr_3$-PET DDPPC film shows

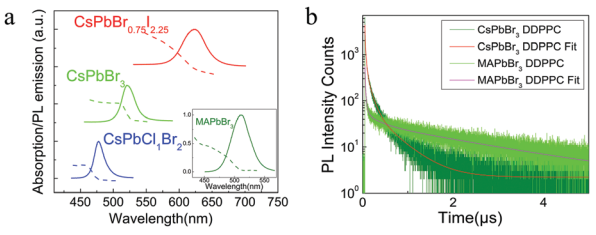

Fig. 2 Optical properties of the synthesized DDPPC films. (a) UV-vis absorption spectra (dotted lines) and PL spectra (solid lines) of DDPPC films with various perovskite compositions. (b) PL decay curves and the corresponding fitting curves of $CsPbBr_3$ and $MAPbBr_3$ DDPPC films.

Table 1 PL emission peaks, FWHMs and the corresponding PLQYs of some DDPPC films

Perovskite components	Emission peaks (nm)	FWHM (nm)	PLQY (%)
$CsPbCl_1Br_2$	477	17.7	2.81
$CsPbBr_3$	520	26.5	45.7
$CsPbBr_{0.75}I_{2.25}$	622	41.8	28.5
$MAPbBr_3$	510	29.8	77.9

τ_{avg} of ~167 ns, which is also much longer than τ_{avg} (50 ns) of the $CsPbBr_3$-PS film prepared by SDM,[56] indicating their outstanding optical quality.

The $CsPbBr_3$, $CsPbBr_{0.75}I_{2.25}$, and $MAPbBr_3$ DDPPC films remain bright after being immersed in water for over 3 years in the ambient environment, as shown in Fig. 3a–c, respectively. To test their thermal stability, the DDPPC films are heated to each set temperature, maintained for a while, and then cooled to room temperature (25 °C) while monitoring the PL spectra. After a 100 °C thermal cycle, the $CsPbBr_{0.75}I_{2.25}$ and $MAPbBr_3$ DDPPC films can fully recover their initial PL intensities (Fig. 3d and e). Even after a 140 °C thermal cycle, $CsPbBr_{0.75}I_{2.25}$ DDPPC film still maintains ~85% of its initial PL intensity (Fig. 3f), and the PL intensity of the $MAPbBr_3$ DDPPC film is fully recovered (Fig. 3g). For the $CsPbBr_3$ DDPPC film, it only maintains ~58% of its original PL intensity after a 100 °C heating cycle (Fig. S16, ESI†), which may be ascribed to concentration quenching at high temperature. During the test, no obvious change in the emission peak and FWHM is observed, indicating a good structural stability under thermal cycles.

To further test the damp-heat stability of the obtained DDPPC films, they are stored in a home-made incubator at high temperature (70 °C) and high humidity (90% Relative humidity, RH) for 30 days, and their corresponding PL intensity is recorded during the test (Fig. 3g). All films show excellent stability under such harsh conditions. For $CsPbBr_3$ and $MAPbBr_3$ DDPPC films, 71.6% and 84.7% of their original PL intensities are conserved, respectively. In the previous SDM-related works, the red PPCs suffer from poor damp-heat survival ability and very dimmed PL emission. Surprisingly, the PL intensity of red $CsPbBr_{0.75}I_{2.25}$ DDPPCs is even slightly enhanced after 60 days in the incubator (Fig. S17, ESI†). In fact, a previous study has demonstrated humidity-enhanced PL of perovskite-polymer composites, and it has been suspected that the hydrogen bonds in water molecules can deactivate the nonradiative recombination centers on the nanocrystals.[37]

The obtained DDPPCs also exhibit excellent light stability under continuous exposure to an intense blue laser (with an irradiance of 100 mW cm^{-2}; the testing setup can be found in Fig. S18, ESI†). After 4 hours of extended testing, the red DDPPC film maintains 50.7% of its original luminescent intensity. Moreover, soon after the excitation is switched off, the emission can quickly (less than 1 minute) recover to 90% of its original intensity. The same setup is utilized to test the photostability of $CsPbBr_3$ and $MAPbBr_3$ DDPPC films. After 10 hours of excitation, 61.6% and 87.6% of their original PL intensity can be maintained for $CsPbBr_3$ and $MAPbBr_3$ DDPPC films,

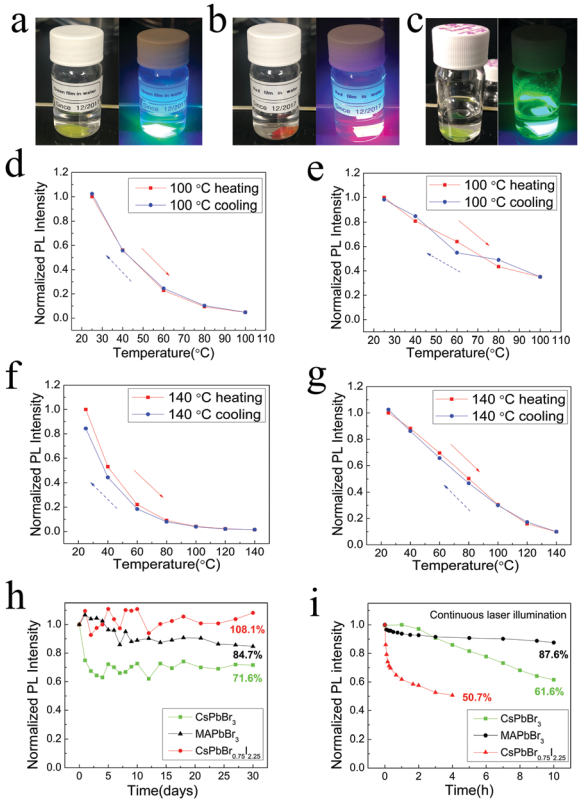

Fig. 3 Water, thermal, photo and damp-heat stability characterizations. (a) $CsPbBr_3$, (b) $CsPbBr_{0.75}I_{2.25}$, and (c) $MAPbBr_3$ DDPPC films immersed in water for three years under ambient environment (left) without visible PL decay by UV excitation (right). (d and e) The 100 °C thermal cycle test results of (d) $CsPbBr_{0.75}I_{2.25}$ and (e) $MAPbBr_3$ DDPPC films. (f and g) The 140 °C thermal cycle test results of (f) $CsPbBr_{0.75}I_{2.25}$ and (g) $MAPbBr_3$ DDPPC films. (h) Relative PL intensity fluctuations of the corresponding DDPPC films during the damp-heat (70 °C, 90 RH) test for 30 days. (i) Photo stability test of DDPPC films under continuous 457 nm blue laser illumination with an irradiance of 100 mW cm^{-2}.

respectively, and their PL intensity is fully recovered once the laser is turned off.

Such impressive water-, thermal-, damp-heat-, and photostability should be attributed to the safeguarding of the inert PET polymer matrix. Since PET is a typical sturdy barrier polymer with high crystallinity, it can prevent small oxygen, water or relevant molecules, which will possibly cause the degradation of the embedded perovskite nanocrystals, from diffusing into the inert polymer matrix.[41,42] Thus, the lifetime of the embedded perovskite NCs is significantly extended.

Because of the simple fabrication process, relatively low cost of the raw materials, ultra-high environmental stability, high PL efficiency and saturated colors of the DDPPCs, they are promising candidates for PL-related applications. Since the films can be easily scaled up as described in Fig. S19 (ESI†), one near-term application would be tunable downconverters for liquid crystal display (LCD) backlights. To demonstrate this concept, red and green DDPPC films are applied as the downconverters and pumped by a blue LED (Fig. 4a). The spectrum of the mixed backlight is depicted in Fig. 4b. Such a backlight

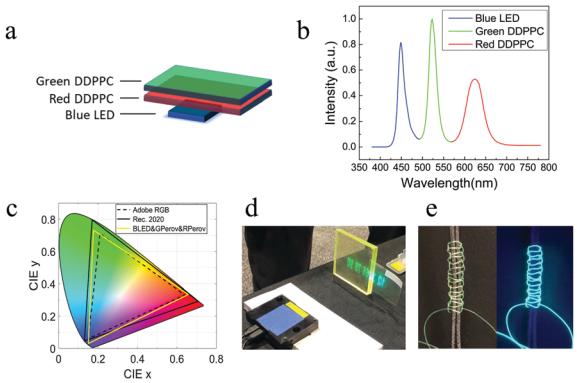

Fig. 4 Application of the ultrastable DDPPCs. (a) Schematic of applying red and green DDPPC films as downconverting sheets in liquid crystal display backlights. (b) Simulated PL emission spectra of a white LED system (D65) with red $CsPbBr_{0.75}I_{2.25}$ and green $CsPbBr_3$-DDPPC films as color conversion layers for blue LEDs. (c) Color gamut coverage of Adobe RGB and Rec. 2020 standards in CIE 1931 color space. (d) The application of the DDPPC film in transparent projection displays. (e) The weaved luminescent DDPPC fibers.

can match the color coordinate of CIE standard illuminant D65, and can successfully cover 99.82% of the adobe RGB color gamut, as well as 81.83% of the Rec. 2020 color gamut (Fig. 4c). The color gamut coverage range can be potentially enhanced by further hybridizing the DDPPC films with other downconverters, such as narrow band phosphors or quantum dots.

Meanwhile, the brightly luminescent composite film with high transparency is an excellent candidate to be used in transparent projection displays.[37,59] As shown in Fig. 4d, a $CsPbBr_3$-PET DDPPC film is inserted between two pieces of glass. Using a UV projector as the excitation light source, images can be formed on the DDPPC film. On the other hand, the luminescent composite fibers (Fig. 4e), due to their excellent mechanical properties, can be weaved or knitted into functional fabrics for luminescent optical fibers or smart texture applications as a demonstration.[60]

3. Conclusions

As a conclusion, we have illustrated a simple, scalable, and cost effective deep-dyeing strategy for luminescent perovskite-polymer composite fabrication. The as-obtained DDPPCs exhibit high optical efficiency up to 77.9%, excellent color purity (FWHM ranging from 18 nm to 42 nm) and tunable wavelengths from 477 nm to 645 nm. Thanks to the protection of the inert PET polymer matrix, superior water-, thermal-, and photostability can be achieved even without further protection of any barrier layers. The deep-dyeing strategy improves the stability of not only pure bromide-based green emitting DDPPCs but also iodine-containing red DDPPCs such that they can survive in water for more than 3 years without noticeable degradation. Further characterizations showed that PL is reversible under thermal treatment, and the PL intensity can be well maintained under continuous blue laser irradiation. Ascribed to their optical properties and environmental stabilities, the DDPPCs

are considered to have great potential to be employed as color conversion materials in various industrial applications, such as display backlight systems, SSL, and luminescent textiles.

Conflicts of interest

There are no conflicts to declare.

Acknowledgements

The authors thank the Materials Characterization Facility AMPAC of the University of Central Florida (UCF) for helping with TEM characterizations and Ted Sun for providing the UV projector for transparent projection display demonstration. Y. Dong is grateful for the support by UCF through startup funding (Grant No. 20080738) and an NSTC seed grant (No. 63014223) for this work. T. L. Chiu would like to thank the support by the Ministry of Science and Technology (MOST), Taiwan, under Grants MOST 109-2622-E-155-014, 108-2221-E-155-051-MY3.

Notes and references

1 Z. He, C. Zhang, Y. Dong and S. T. Wu, *Crystals*, 2019, **9**, 59.
2 H. Chen, J. H. Lee, B. Y. Lin, S. Chen and S. T. Wu, *Light: Sci. Appl.*, 2018, **7**, 17168.
3 K. Masaoka, Y. Nishida, M. Sugawara and E. Nakasu, *IEEE Trans. Broadcast.*, 2010, **56**, 452.
4 P. M. Pattison, J. Y. Tsao, G. C. Brainard and B. Bugbee, *Nature*, 2018, **563**, 493–500.
5 J. K. Kim, H. Luo, E. F. Schubert, J. Cho, C. Sone and Y. Park, *Jpn. J. Appl. Phys.*, 2005, **44**, 649.
6 A. Bergh, G. Craford, A. Duggal and R. Haitz, *Phys. Today*, 2001, **54**, 42.
7 G. Singh and D. S. Mehta, *J. Inf. Disp.*, 2014, **15**, 91.
8 Z. Luo, D. Xu and S. T. Wu, *J. Disp. Technol.*, 2014, **10**, 526.
9 J. H. Oh, S. J. Yang and Y. R. Do, *Light: Sci. Appl.*, 2014, **3**, e141.
10 R. Zhu, Z. Luo, H. Chen, Y. Dong and S. T. Wu, *Opt. Express*, 2015, **23**, 23680.
11 H. Ji, H. Xu, F. Jiang, Z. Bai and H. Zhong, *SID Int. Symp. Dig. Tech. Pap.*, 2019, **50**, 411.
12 Q. Zhou, Z. Bai, W. Lu, Y. Wang, B. Zou and H. Zhong, *Adv. Mater.*, 2016, **28**, 9163.
13 J. V. Derlofske, J. Schumacher, J. Hillis, D. Lamb, F. McCormick and A. Lathrop, *Quantum Dot Enchancement Film (QDEF)*, 3M White Paper, 2013.
14 M. C. Leung, *White LED and Remote Phosphor Comparison*, Cree White Paper, 2014.
15 B. Xie, R. Hu and X. Luo, *J. Electron. Packag.*, 2016, **138**, 020803.
16 S. D. Stranks and H. J. Snaith, *Nat. Nanotechnol.*, 2015, **10**, 391.
17 C. M. MacLaughlin, *ACS Energy Lett.*, 2019, **4**, 977.
18 H. Cho, S. H. Jeong, M. H. Park, Y. H. Kim, C. Wolf, C. L. Lee, J. H. Heo, A. Sahanala, N. Myoung, S. Yoo, S. H. Im, R. H. Friend and T. W. Lee, *Science*, 2015, **350**, 1222.
19 L. Protesescu, S. Yakunin, M. I. Bodnarchuk, F. Krieg, R. Caputo, C. H. Hendon, R. X. Yang, A. Walsh and M. V. Kovalenko, *Nano Lett.*, 2015, **15**, 3692.
20 F. Zhang, H. Z. Zhong, C. Chen, X. G. Wu, X. M. Hu, H. L. Huang, J. B. Han, B. S. Zou and Y. P. Dong, *ACS Nano*, 2015, **9**, 4533.
21 I. Levchuk, A. Osvet, X. Tang, M. Brandl, J. D. Perea, F. Hoegl, G. J. Matt, R. Hock, M. Batentschuk and C. J. Brabec, *Nano Lett.*, 2017, **17**, 2765.
22 A. Swarnkar, R. Chulliyil, V. K. Ravi, M. Irfanullah, A. Chowdhury and A. Nag, *Angew. Chem.*, 2015, **127**, 15644.
23 C. Zhang, Z. He, H. Chen, L. Zhou, G. Tan, S. T. Wu and Y. Dong, *J. Mater. Chem. C*, 2019, **7**, 6527.
24 D. W. de Quilettes, S. M. Vorpahl, S. D. Stranks, H. Nagaoka, G. E. Eperon, M. E. Ziffer, H. J. Snaith and D. S. Ginger, *Science*, 2015, **348**, 683.
25 J. Berry, T. Buonassisi, D. A. Egger, G. Hodes, L. Kronik, Y. L. Loo, I. Lubomirsky, S. R. Marder, Y. Mastai, J. S. Miller, D. B. Mitzi, Y. Paz, A. M. Rappe, I. Riess, B. Rybtchinski, O. Stafsudd, V. Stevanovic, M. F. Toney, D. Zitoun, A. Kahn, D. Ginley and D. Cahen, *Adv. Mater.*, 2015, **27**, 5102.
26 S. Brittman and J. Luo, *Nano Lett.*, 2018, **18**, 2747.
27 B. Conings, J. Drijkoningen, N. Gauquelin, A. Babayigit, J. D'Haen, L. D'Olieslaeger, A. Ethirajan, J. Verbeeck, J. Manca, E. Mosconi, F. D. Angelis and H. G. Boyen, *Adv. Energy Mater.*, 2015, **5**, 1500477.
28 Y. Wei, Z. Cheng and J. Lin, *Chem. Soc. Rev.*, 2019, **48**, 310.
29 H. Liao, S. Guo, S. Cao, L. Wang, F. Gao, Z. Yang, J. Zheng and W. Yang, *Adv. Opt. Mater.*, 2018, **6**, 1800346.
30 L. Xu, J. Chen, J. Song, J. Li, J. Xue, Y. Dong, B. Cai, Q. Shan, B. Han and H. Zeng, *ACS Appl. Mater. Interfaces*, 2017, **9**, 26556.
31 M. Meyns, M. Perálvarez, A. Heuer-Jungemann, W. Hertog, M. Ibáñez, R. Nafria, A. Genç, J. Arbiol, M. V. Kovalenko, J. Carreras, A. Cabot and A. G. Kanaras, *ACS Appl. Mater. Interfaces*, 2016, **8**, 19579.
32 H. Zhang, X. Wang, Q. Liao, Z. Xu, H. Li, L. Zheng and H. Fu, *Adv. Funct. Mater.*, 2017, **27**, 1604382.
33 Y. Wang, J. He, H. Chen, J. Chen, R. Zhu, P. Ma, A. Towers, Y. Lin, A. J. Gesquiere, S. T. Wu and Y. Dong, *Adv. Mater.*, 2016, **28**, 10710.
34 Z. He, J. He, C. Zhang, S. T. Wu and Y. Dong, *Chem. Rec.*, 2020, **20**, 672.
35 L. J. Xu, M. Worku, H. Lin, Z. Xu, Q. He, C. Zhou, H. Zhang, Y. Xin, S. Lteif, J. Xue and B. Ma, *J. Phys. Chem. Lett.*, 2019, **10**, 5923.
36 B. Luo, Y.-C. Pu, S. A. Lindley, Y. Yang, L. Lu, Y. Li, X. Li and J. Z. Zhang, *Angew. Chem., Int. Ed.*, 2016, **55**, 8864.
37 J. He, Z. He, A. Towers, T. Zhan, H. Chen, L. Zhou, C. Zhang, R. Chen, T. Sun, A. J. Gesquiere, S. T. Wu and Y. Dong, *Nanoscale Adv.*, 2020, **2**, 2034.
38 S. Chang, Z. Bai and H. Zhong, *Adv. Opt. Mater.*, 2018, **6**, 1800380.
39 B. Luo, S. B. Naghadeh and J. Zhang, *ChemNanoMat*, 2017, **3**, 456.

40 L. Protesescu, S. Yakunin, S. Kumar, J. Bar, F. Bertolotti, N. Masciocchi, A. Guagliardi, M. Grotevent, I. Shorubalko, M. I. Bodnarchuk, C. J. Shih and M. V. Kovalenko, *ACS Nano*, 2017, **11**, 3119.
41 P. E. Keller and R. T. Kouzes, *Water Vapor Permeation in Plastics*, Pacific Northwest National Laboratory, Richland, WA, 2017.
42 V. Siracusa, *Int. J. Polym. Sci.*, 2012, **2012**, 302029.
43 M. Kinami, B. R. Crenshaw and C. Weder, *Chem. Mater.*, 2006, **18**, 946.
44 http://www.campoly.com/files/3013/5216/6056/005.pdf.
45 S. Nandi and H. H. Winter, *Macromolecules*, 2005, **38**, 4447.
46 P. J. Flory and J. Rehner, *J. Chem. Phys.*, 1943, **11**, 521.
47 K. Elnagar, T. A. Elmaaty and S. Raouf, *J. Text.*, 2014, 363079.
48 S. Fu, D. Hinks, P. J. Hauser and M. A. Ankeny, *Cellulose*, 2013, **20**, 3101.
49 X. Xiong, Y. Xu, L. Zheng, J. Yan, H. Zhao, J. Zhang and Y. Sun, *J. Fluoresc.*, 2017, **27**, 483.
50 X. Liu, Y. Ning and F. Wang, *Color Res. Appl.*, 2014, **39**, 511.
51 X. Yang and R. B. Turner, *U.S. Patent*, 6,652,602, Washington, DC, 2003.
52 E. A. Mercado, *U.S. Patent*, 5,162,046, Washington, DC, 1992.
53 E. A. Mercado, *U.S. Patent*, 5,338,318, Washington, DC, 1994.
54 C. Zhang, Z. He, C. Gao, S. T. Wu and Y. Dong, *SID Int. Symp. Dig. Tech. Pap.*, 2020, **51**, 1303.
55 K. M. Lee, C. J. Lin, B. Y. Liou, S. M. Yu, C. C. Hsu, V. Suryanarayanan and M. C. Wu, *Sol. Energy Mater. Sol. Cells*, 2017, **172**, 368.
56 J. A. Sichert, Y. Tong, N. Mutz, M. Vollmer, S. Fischer, K. Z. Milowska, R. García Cortadella, B. Nickel, C. Cardenas-Daw, J. K. Stolarczyk, A. S. Urban and J. Feldmann, *Nano Lett.*, 2015, **15**, 6521.
57 H. Xiao, Y. Wei, P. Dang, S. Liang, Z. Cheng, G. Li and J. Lin, *J. Mater. Chem. C*, 2020, **8**, 9968.
58 D. W. deQuilettes, S. Koch, S. Burke, R. K. Paranji, A. J. Shropshire, M. E. Ziffer and D. S. Ginger, *ACS Energy Lett.*, 2016, **1**, 438.
59 T. X. Sun, *Inf. Disp.*, 2020, **36**, 21.
60 W. Ding, J. Sun, G. Chen, L. Zhou, J. Wang, X. Gu, J. Wan, X. Pu, B. Tang and Z. L. Wang, *J. Mater. Chem. C*, 2019, **7**, 10769.

